Title

Multiphase Chemical Kinetics of OH Radical Uptake by Molecular Organic Markers of Biomass Burning Aerosols: Humidity and Temperature Dependence, Surface Reaction, and Bulk Diffusion

Journal

The Journal of Physical Chemistry A, 119(19)

ISSN

1089-5639

Authors

Arangio, Andrea M
Slade, Jonathan H
Berkemeier, Thomas
et al.

Publication Date

2015-05-14

DOI

10.1021/jp510489z

Peer reviewed

THE JOURNAL OF PHYSICAL CHEMISTRY A

Article

pubs.acs.org/JPCA

Multiphase Chemical Kinetics of OH Radical Uptake by Molecular Organic Markers of Biomass Burning Aerosols: Humidity and Temperature Dependence, Surface Reaction, and Bulk Diffusion

Andrea M. Arangio,[†] Jonathan H. Slade,[‡] Thomas Berkemeier,[†] Ulrich Pöschl,[†] Daniel A. Knopf,*[,‡] and Manabu Shiraiwa*[,†]

[†]Multiphase Chemistry Department, Max Planck Institute for Chemistry, D-55128 Mainz, Germany

[‡]Institute for Terrestrial and Planetary Atmospheres, School of Marine and Atmospheric Sciences, Stony Brook University, Stony Brook, New York 11794, United States

ABSTRACT: Multiphase reactions of OH radicals are among the most important pathways of chemical aging of organic aerosols in the atmosphere. Reactive uptake of OH by organic compounds has been observed in a number of studies, but the kinetics of mass transport and chemical reaction are still not fully understood. Here we apply the kinetic multilayer model of gas−particle interactions (KM-GAP) to experimental data from OH exposure studies of levoglucosan and abietic acid, which serve as surrogates and molecular markers of biomass burning aerosol (BBA). The model accounts for gas-phase diffusion within a cylindrical coated-wall flow tube, reversible adsorption of OH, surface-bulk exchange, bulk diffusion, and chemical reactions at the surface and in the bulk of the condensed phase. The nonlinear dependence of OH uptake coefficients on reactant concentrations and time can be reproduced by KM-GAP. We find that the bulk diffusion coefficient of the organic molecules is approximately 10^{-16} cm^2 s^{-1}, reflecting an amorphous semisolid state of the organic substrates. The OH uptake is governed by reaction at or near the surface and can be kinetically limited by surface-bulk exchange or bulk diffusion of the organic reactants. Estimates of the chemical half-life of levoglucosan in 200 nm particles in a biomass burning plume increase from 1 day at high relative humidity to 1 week under dry conditions. In BBA particles transported to the free troposphere, the chemical half-life of levoglucosan can exceed 1 month due to slow bulk diffusion in a glassy matrix at low temperature.

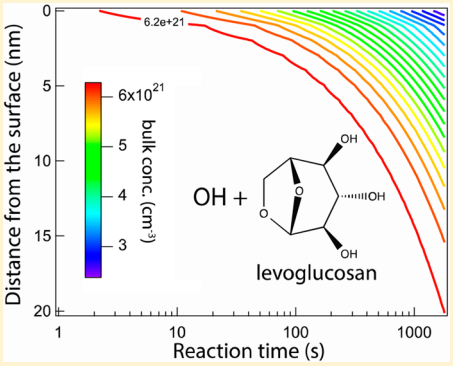

INTRODUCTION

Biomass burning is one of the largest sources of primary organic aerosols, black carbon,[1] and trace gases in the Earth's atmosphere with a source strength comparable to fossil fuel burning.[2−4] Biomass burning aerosol (BBA) has a significant impact on climate and public health. BBAs are ubiquitous and via pyro-convection can also reach the upper troposphere and lower stratosphere regions of the atmosphere.[5−9] They scatter or absorb solar radiation and can serve as cloud condensation nuclei and ice nuclei affecting cloud microphysical and radiative properties.[10,11] Black and brown carbon produced from incomplete combustion are important contributors to the radiative forcing,[12,13] and polycyclic aromatic hydrocarbons (PAHs) associated with BBA can cause adverse health effects such as oxidative stress.[14−16]

Several field campaigns and remote sensing studies have been performed to investigate the impact of biomass burning on local, regional, and global scales.[17−21] The contribution of biomass burning emissions to field-collected particles is typically evaluated by applying chemical receptor-based models, which utilize source-specific molecules, also termed biomolecular markers, found in the particles to identify the source and estimate aerosol source strength.[22] Levoglucosan (1,6-anhydro-β-D-glucopyranose, $C_6H_{10}O_5$) and abietic acid (1-phenanthrenecarboxylic acid, $C_{20}H_{30}O_2$) are produced during lignin and hemicellulose combustion and often used as molecular markers of biomass burning emission.[23−25]

Although levoglucosan and abietic acid are considered chemically stable in the atmosphere, several field campaigns on BBA emissions have shown large seasonal variations of levoglucosan concentration characterized by a strong levoglucosan depletion during summer compared to C/O ratio and K^+, which indicates the marker's degradation during transport.[26,27] This is supported by laboratory studies which have shown that levoglucosan and abietic acid can degrade by photooxidation[28] and heterogeneous reactions with OH[29−35] and NO_3 radicals.[36,37] The reaction rate of the marker depends on the gas-phase concentration of the oxidants[29] as well as relative humidity (RH).[35] Multiphase chemical processes alter the physical and chemical properties of the particles,[38−41] which in turn impact radiative and hygroscopic properties, cloud

Special Issue: Mario Molina Festschrift

Received: October 18, 2014
Revised: February 13, 2015
Published: February 16, 2015

DOI: 10.1021/jp510489z
J. Phys. Chem. A 2015, 119, 4533−4544

condensation nuclei and ice nuclei activities,[42−44] brown carbon formation,[45−47] and toxicity.[16,48] Multiphase oxidation of levoglucosan and abietic acid by OH can also lead to significant degradation.[29−33,35]

In experimental studies heterogeneous and multiphase chemical processes are often characterized by the uptake coefficient γ_{OH}, which is the ratio between the net flux of OH to the particle and the OH collision flux.[49] The γ_{OH} values experimentally derived for levoglucosan and abietic acid reacting with OH are in the range of 0.056−1.[29,35] Applying the kinetic multilayer model of gas−particle interactions in aerosols and clouds (KM-GAP),[50] we analyze new experimental data on the OH exposure of levoglucosan and abietic acid substrates under dry conditions and investigate the relative contributions of surface and bulk reactions to the overall OH uptake. KM-GAP allows us to estimate kinetic parameters such as surface accommodation coefficient, desorption time, reaction rate coefficients, bulk diffusion coefficients of both OH and organics, and the Henry's law coefficient of OH in the organic phase. Kinetic regimes and limiting cases[51,52] of the multiphase reactions of OH radicals were investigated by systematic sensitivity studies to the laboratory data. Finally, the chemical half-life of levoglucosan due to heterogeneous and multiphase reactions was estimated for atmospherically relevant gas-phase OH concentrations.

METHODS

Figure 1 shows a schematic of the KM-GAP model with multiple compartments and layers: gas phase, near-surface gas phase, sorption layer, surface layer, and a number of bulk layers. KM-GAP treats the following processes of mass transport and chemical reactions explicitly: gas-phase diffusion, surface adsorption and desorption, surface-bulk exchange, bulk diffusion, and chemical reactions at the surface and in the bulk.[50] Gas-phase diffusion flux and correction factor for a cylindrical flow tube are derived analogous to spherical particles as described in Pöschl et al. (2007)[49] and has been validated[53] against the numerical approach of Brown,[54] which had also been used to determine the experimental γ_{OH} values.[29] Surface and bulk layer thicknesses can change due to volatilization or condensation in response to mass transport, which eventually leads to particle growth or shrinkage. Mass transport fluxes between layers are based on the first-order approximation of Fick's diffusion equation using bulk diffusion coefficients.[50] The surface-bulk exchange is constrained by solubility of the compound in the bulk (e.g., by the Henry's law coefficient). For the simulation of coated-wall flow-tube experiments, the initial thickness of the organic film was taken to be 100 nm and described by 100 model layers. The exact number of model layers was relevant for the resolution of the bulk profile but not for the overall model result of OH uptake, which was determined by chemical reaction in the uppermost few nanometers of the organic film. Like in the determination of experimental γ_{OH} values,[29] the organic surface was assumed to be smooth. For the estimation of chemical half-lifes and the degraded fraction of biomass burning particles, we assumed spherical geometry of the particles.

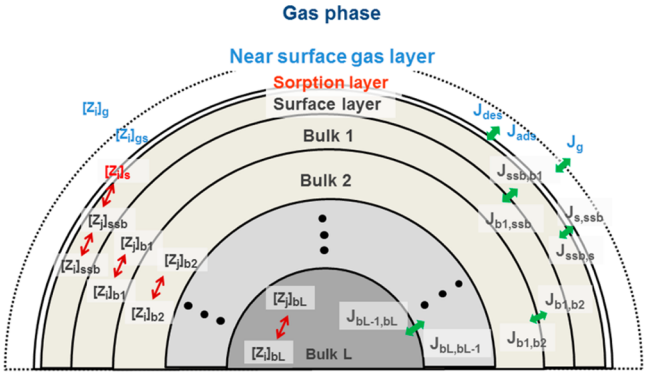

Figure 1. Schematics of the kinetic multilayer model of gas−particle interactions in aerosols and clouds (KM-GAP).[50] Concentrations of species Z_i and Z_j in the gas (g) and near-surface gas phase, at the sorption layer (s) and in the surface (ssb) and in the bulk (b) layers. J are the transport fluxes between each layer, including the gas-phase diffusion flux (J_g), the adsorption (J_{ads}) and desorption (J_{des}) fluxes, surface−bulk exchange fluxes ($J_{s,ssb}$, $J_{ssb,s}$), and bulk diffusion fluxes (J_b).

The reaction rates at the surface and in the bulk are described using a second-order dependence from the concentration of the reactants in each bulk layer. The reaction scheme for levoglucosan and abietic acid reacting with OH was proposed by Slade and Knopf.[29] Hydrogen abstraction from the substrate is the first and the limiting step for both levoglucosan and abietic acid, as also suggested by molecular dynamic simulations.[55] Two reaction products are considered in the model, one being volatile and the other nonvolatile. For simplicity, secondary reactions between OH and these products are not taken into account; these are usually slower than the primary reaction.[56] Self-reaction of OH on the surface is also neglected because the uptake coefficients reported for OH self-reaction are as low as 10^{-4}.[29,57]

The temporal evolution of the uptake coefficient, γ_{OH}, and the surface and bulk compositions were simulated by numerically solving the ordinary differential equations considering the mass balance of each layer. The physically well-constrained input parameters include thermal velocity of OH (T = 298 K; ω_{OH} = 6.1 × 10^4 cm s^{-1}), effective molecular diameter of OH (δ_{OH} = 0.30 nm), levoglucosan (LG; δ_{LG}= 0.69 nm), and abietic acid (AA; δ_{AA} = 0.78 nm).[37] The gas-phase diffusion coefficient of OH under experimental conditions was 185 cm^2 s^{-1}.[29] The concentration of levoglucosan for each bulk layer is 6.27 × 10^{21} cm^{-3} considering a densely packed system formed exclusively by levoglucosan molecules (molecular volume =1.59 × 10^{-22} cm^3).[37]

The kinetic input parameters include the surface accommodation coefficient of OH on a free substrate ($\alpha_{s,0}$), desorption lifetime (τ_d), second-order surface (k_{SLR}) and bulk (k_{BR}) reaction rate coefficients between OH and organics, Henry's law coefficient of OH ($K_{sol,cc}$) in the organic phase, and the bulk diffusion coefficients for OH and organics (D_{OH}, D_{org}), respectively. We assumed $\alpha_{s,0}$ = 1, as the measured maximum γ_{OH} for this reaction system is ∼0.9,[29,35] and $\alpha_{s,0}$ needs to be larger than γ_{OH} by definition.[49] This assumption is also consistent with molecular dynamic simulations of OH[58] and our previous study on kinetic modeling and experiments of ozonolysis on organic surfaces.[48] Moreover, sensitivity studies showed that the modeled γ_{OH} is insensitive to $\alpha_{s,0}$ as long as $\alpha_{s,0}$ >∼0.5. Other parameters are less constrained and used as fitting parameters in this study.

To fit the experimental data, we varied the kinetic parameters in KM-GAP using a global optimization method that utilizes a uniformly sampled Monte Carlo search to seed a genetic algorithm (MCGA method). The genetic algorithm (Matlab

DOI: 10.1021/jp510489z
J. Phys. Chem. A 2015, 119, 4533−4544

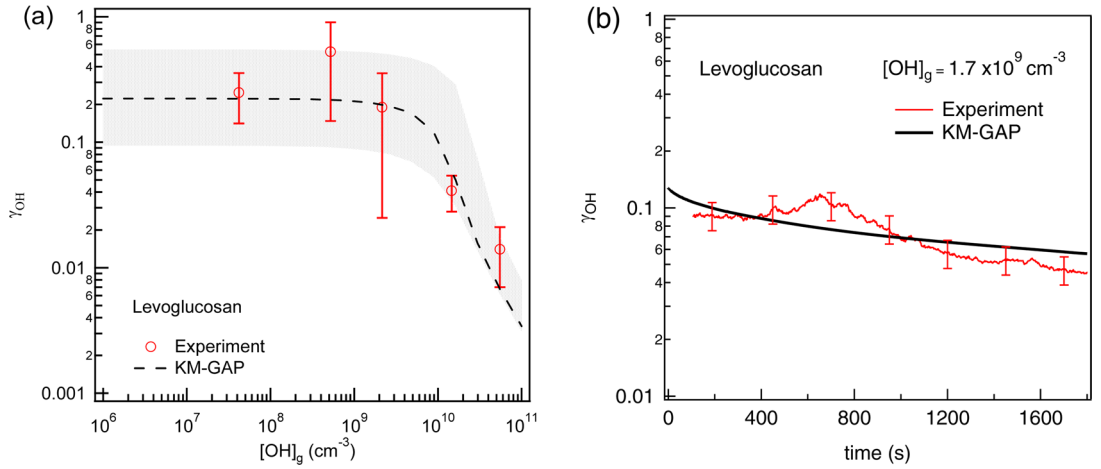

Figure 2. OH uptake coefficient (γ_{OH}) for levoglucosan measured (red) and modeled (black) by KM-GAP. (a) γ_{OH} as a function of gas-phase OH concentration. The shaded area represents model simulations with different sets of kinetic parameters determined by the Monte Carlo genetic algorithm method. (b) Temporal evolution of γ_{OH} with gas-phase OH concentration of 1.7 × 10^9 cm^{-3}.

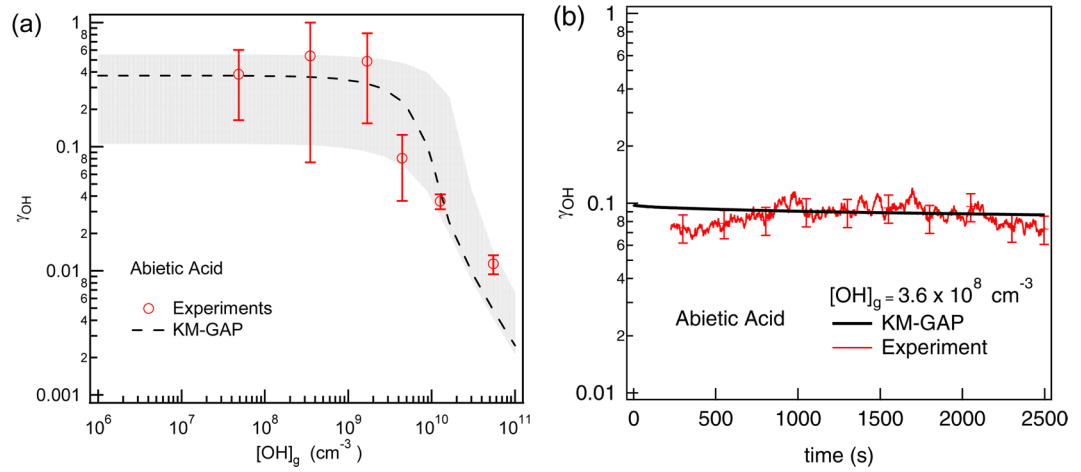

Figure 3. OH uptake coefficient (γ_{OH}) for abietic acid measured (red) and modeled (black) by KM-GAP. (a) γ_{OH} as a function of gas-phase OH concentration. The shaded area represents model simulations with different sets of kinetic parameters determined by the Monte Carlo genetic algorithm method. (b) Temporal evolution of γ_{OH} with gas-phase OH concentration of 3.6 × 10^8 cm^{-3}.

software) was terminated when the correlation between experimental data and model output converged into an optimum. Since the optimization of the kinetic parameters to the experimental data was not unique in all kinetic parameters, repeated execution of the MCGA method yields a range of kinetic parameters, which can be used to describe the experimental data. For each parameter a plausible range of variation was chosen based on previous kinetic studies.[37,48,50,51,59,60] The upper limit of k_{BR} is given by the rate coefficient of a diffusion-controlled reaction which can be estimated from the bulk diffusion coefficients and effective molecular radii of the reactants:[61]

$$k_{BR,max} = 4\pi(D_{OH} + D_{org})(r_{OH} + r_{org})$$

Assuming $r_{OH} + r_{org} \approx r_{org} \approx 10^{-7}$ cm, we obtain $k_{BR,max} \approx 10^{-11}$ cm^3 s^{-1} for a liquid matrix with $D_{OH} + D_{org} \approx D_{OH} \approx 10^{-5}$ cm^2 s^{-1} and $k_{BR,max} \approx 10^{-14}$ cm^3 s^{-1} for a semisolid matrix with $D_{OH} + D_{org} \approx D_{OH} \approx 10^{-8}$ cm^2 s^{-1}. Earlier studies have reported a range of 3.1 × 10^{-13} to 1.1 × 10^{-11} cm^3 s^{-1} for the bulk reaction rate coefficient of OH and levoglucosan in the liquid phase,[28,30,32,33] but no literature values are available for semisolid or solid phases. Assuming that the kinetics of diffusion and reaction at the surface are similar to the bulk, a rough estimate for the upper limit of the surface reaction rate coefficient can be obtained by dividing the maximum bulk rate coefficient through the sum of the effective molecular radii of the reactants (~10^{-7} cm), yielding $k_{SLR,max} \sim 10^{-4}$ cm^2 s^{-1}. Note, however, that the maximum rates of surface diffusion and reaction may substantially deviate from the bulk-derived estimates depending on the reaction system and conditions.[62,63]

Levoglucosan and abietic acid substrates were exposed under dry conditions to OH in the presence of O_2 using a coated-wall flow-tube reactor coupled to a chemical ionization mass spectrometer as described in detail previously.[29] In brief, OH radicals were produced via a microwave discharge of H_2 in a He carrier flow followed by reaction with O_2 in a movable halocarbon wax-coated glass injector.[57] OH was detected as OH^- following chemical ionization by SF_6^-. OH radical concentrations in these experiments varied from ~10^8 to 10^9 molecules cm^{-3}, representing, within an order of magnitude, concentrations measured in fresh biomass burning plumes.[64] The organic substrates were exposed to OH radicals for about ~40 min at about 5.5 hPa. The residence time for OH over the exposed substrate ranged from 0.08 to 1.25 ms. Uptake

DOI: 10.1021/jp510489z
J. Phys. Chem. A 2015, 119, 4533−4544

coefficients were derived experimentally as described in detail previously[36] and corrected for gas-phase diffusion to the flow reactor walls by application of the Brown formalism.[54]

RESULTS AND DISCUSSION

Figures 2a and 3a show γ_{OH} as a function of gas-phase OH concentration, $[OH]_g$, for levoglucosan and abietic acid, respectively. γ_{OH} for levoglucosan and abietic acid stays constant at ~0.3 when $[OH]_g$ is below ~10^9 cm^{-3}. Above this concentration, γ_{OH} decreases to ~0.01 at $[OH]_g = 10^{11}$ cm^{-3}. The temporal evolution of γ_{OH} for levoglucosan and abietic acid at $[OH]_g = 1.7 \times 10^9$ cm^{-3} and 3.6×10^8 cm^{-3}, respectively, are shown in Figures 2b and 3b, respectively. For levoglucosan, γ_{OH} shows a slight decrease from ~0.1 to ~0.06 during the reaction time of 1800 s. The slight increase of the uptake coefficient after ~500 s is within the range of experimental uncertainties (±17%). For abietic acid, γ_{OH} is stable at ~0.09. As demonstrated by the black lines in Figures 2 and 3, both the time and concentration dependence of γ_{OH} can be reproduced by KM-GAP.

Figure 4 shows the distribution of kinetic parameter values obtained by the MCGA method for levoglucosan and abietic acid. The bulk diffusivities of the organic molecules (D_{org}) are the most tightly constrained parameters, which are found to be ~2×10^{-16} cm^2 s^{-1} for levoglucosan and ~9×10^{-17} cm^2 s^{-1} for abietic acid. It reflects the semisolid nature of the compounds under these experimental conditions as also reported in previous studies[59,65−67] and discussed later with regard to atmospheric implications. Note that the bulk diffusivities derived from the MCGA fitting to the chemical kinetics data are characteristic for the near-surface-bulk region where reactions mainly occur in the investigated systems and diffusivity might be enhanced relative to the inner bulk material.[68] The estimated D_{org} is about 4 orders of magnitude higher than D_{org} assumed in our previous work investigating NO_3 uptake by levoglucosan and abietic acid, in which D_{org} was less well constrained.[37] The MCGA estimates for D_{OH} in levoglucosan and abietic acid range from 10^{-11} to 10^{-8} cm^2 s^{-1}. Price et al.[66] measured the bulk diffusivity of water in levoglucosan as ~10^{-10} cm^2 s^{-1} at 20% RH; we adopt this value for further simulations based on the analogy of gas-phase diffusivity between OH and H_2O.[69]

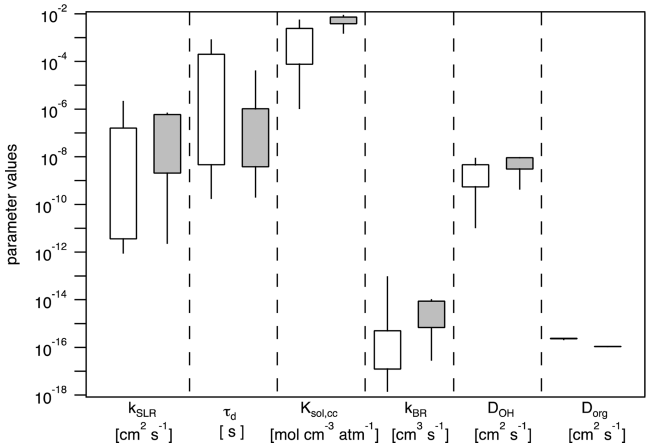

Figure 4. Kinetic parameters for multiphase chemical reactions of OH with levoglucosan (white) and abietic acid (gray) determined by the MCGA method of fitting the experimental data with the KM-GAP model. The ranges of parameters are depicted as a box−whisker plot (the percentiles of 10, 25, 75, and 90% are shown).

For the Henry's law coefficient of OH in the organic phase we obtain a range of 10^{-5}−10^{-3} mol cm^{-3} atm^{-1}, which is at least 1 order of magnitude smaller than that in water.[70−72] The bulk reaction rate coefficient, k_{BR}, is not well constrained with the current experimental data set. Sensitivity analyses indicate that the k_{BR} value does not play a critical role under these experimental conditions and therefore cannot be pinned down by fitting to the experimental data. k_{SLR} and τ_d are found to be mutually interdependent and exhibit a tight inverse correlation as shown in Figure 5. Different combinations of k_{SLR} and τ_d can be chosen due to the wide range of values spanning 7 orders of magnitude. Molecular dynamic simulations[58] suggest that τ_d should be on the order of nanoseconds; if τ_d = 10 ns, then k_{SLR} is constrained to ~10^{-8} cm^2 s^{-1}. This result is consistent with the combination of k_{SLR} ~10^{-10} cm^2 s^{-1} and τ_d ~10 ns used to model the NO_3 uptake by the same organic species in an earlier study,[37] because OH is more reactive than NO_3.

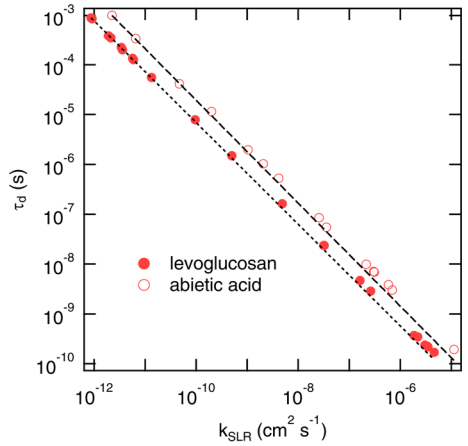

Figure 5. Correlation between desorption lifetime of OH_3 (τ_d) and second-order surface reaction rate coefficients (k_{SLR}) between OH_3 and levoglucosan (solid circles) or abietic acid (open circles) determined by the MCGA method of fitting the experimental data with the KM-GAP model. The black lines are linear fits in a log−log plot.

In evaluating the potential impacts of secondary chemistry on γ_{OH}, we consider reactions between OH and nonvolatile oxidation products applying k_{BR} 2 orders of magnitude smaller than k_{BR} for OH and levoglucosan. The results show that effects of secondary chemistry on γ_{OH} is negligible over the experimental exposure time for $[OH]_g < 10^{10}$ cm^{-3}, while secondary chemistry can affect γ_{OH} for $[OH]_g > 10^{10}$ cm^{-3} by up to 50% only in long exposure time. As k_{BR} for secondary chemistry cannot be constrained well with the current data set, we do not include secondary chemistry for further simulations, although secondary chemistry can be important for the long-term evolution of the condensed phase.[56,73]

Figure 6a shows the temporal evolution of γ_{OH} simulated by KM-GAP, when levoglucosan is exposed to five different OH concentrations (5×10^6 to 5×10^{10} cm^{-3}). For identification of the limiting step for the overall OH uptake, we determine kinetic regimes and limiting cases of the system. Note that the behavior and sensitivity of levoglucosan and abietic acid are very similar; thus, the analysis of only levoglucosan is shown.

DOI: 10.1021/jp510489z
J. Phys. Chem. A 2015, 119, 4533−4544

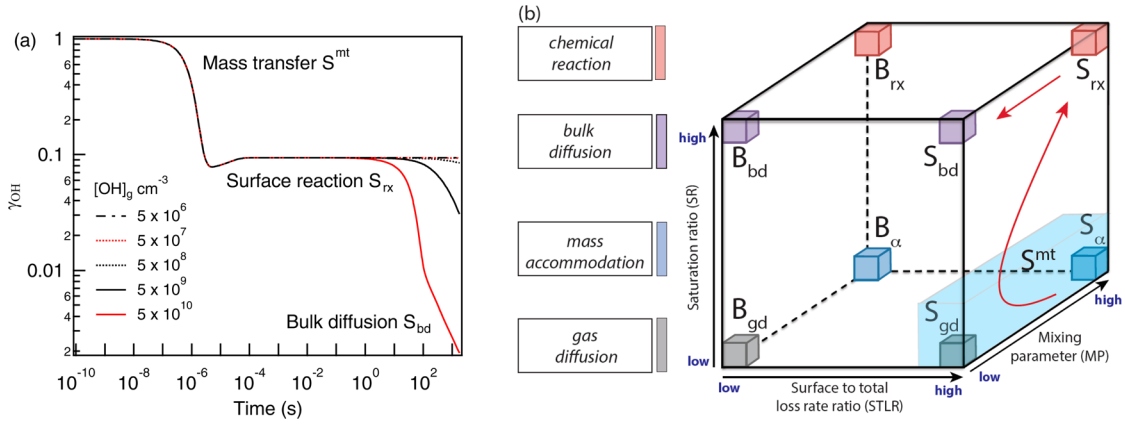

Figure 6. (a) Temporal evolution of OH uptake coefficient (γ_{OH}) for levoglucosan at different OH concentrations. OH uptake is initially limited by mass transfer (S^{mt}) of OH until ~10^{-6} s and then limited by surface reaction (S_{rx}) and the bulk-to-surface transport of levoglucosan (S_{bd}) depending on OH gas-phase concentration. (b) Kinetic regimes and limiting cases of OH uptake are mapped onto the axes of a cube representing reaction location, saturation ratio, and mixing parameter.[51] The red arrows represent evolution of the kinetic regimes: $S^{mt} \rightarrow S_{rx} \rightarrow S_{bd}$.

The cases of limiting behavior arise from the following three criteria that are fundamental to reactive gas uptake:[51,52]

(a) Surface-to-total loss rate ratio (STLR) distinguishes the reaction location between the particle surface (STLR ≈ 1) and the bulk (STLR ≈ 0).

(b) Saturation ratio (SR) determines the abundance of OH at the particle surface or in the bulk. SR ≈ 1 indicates the system is adequately supplied with OH, and SR ≈ 0 indicates the system is deprived of OH and is mass transfer limited.

(c) Mixing parameter (MP) reveals the heterogeneity of the system. MP ≈ 1 indicates the system is well-mixed, and MP ≈ 0 indicates that a strong concentration gradient exists due to diffusion limitation.

The kinetic regimes and limiting cases defined by these criteria can be visualized on a "kinetic cube", in which each axis corresponds to one of the three classification parameters,[51] as shown in Figure 6b. The symbols "S" and "B" indicate the predominant reaction location: particle surface and particle bulk, respectively. A subscript denotes the rate-limiting process for gas uptake: "rx" indicates chemical reaction; "bd" indicates bulk diffusion; "α" indicates mass accommodation; "gd" indicates gas-phase diffusion.

Figure 7 shows the evolution of these criteria at $[OH]_g = 5 \times 10^{10}$ cm^{-3}, and Table 1 summarizes the values for these three criteria for three different time regimes. At any simulated OH concentration, STLR is close to 1 at any simulation time, indicating that the reaction mainly takes place at the particle surface and the system is in the surface reaction regime (S). At the beginning of the uptake process up to ~10^{-6} s, SR at the particle surface (surface saturation ratio; SSR) is very low, indicating that the surface is deprived of OH. γ_{OH} is equal to the surface accommodation coefficient and gas-phase diffusion correction factor (i.e., the ratio of gas-phase concentration at the near-surface gas phase to that far from the surface) is 1 at the very beginning and reduced to ~0.3, implying that mass transfer is the limiting step (S^{mt}) for initial OH uptake.

As shown in Figure 7, SSR becomes ~0.9 after ~10^{-6} s, indicating that the adsorption−desorption equilibrium is established and the surface is close to saturation by OH radicals with respect to a Langmuir adsorption isotherm. Note that the actual surface coverage of OH stays as low as 10^{-6}. The surface mixing parameter of organics (SMP_Y; the ratio of the actual surface concentration to the maximum possible surface

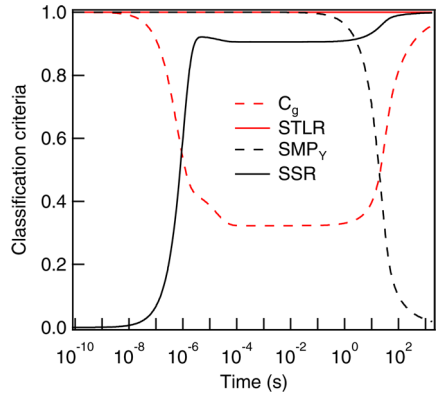

Figure 7. Temporal evolution of criterion parameters for determination of kinetic regimes and limiting cases for multiphase reactions of levoglucosan with $[OH]_g$ of 5×10^{10} cm^{-3}: Surface-to-total loss rate ratio (STLR), gas-phase diffusion correction factor (C_g), surface saturation ratio (SSR), and surface mixing parameter (SMP).

Table 1. Assignment of Kinetic Regimes and Limiting Cases for Multiphase Chemical Reactions of OH with Levoglucosan

	<10^{-6} s	10^{-6}–1 s	1–10^3 s
STLR	~1	~1	~1
SSR	~0	~0.9	~0.9–1
SMP_Y	~1	~1	~0.02–1
kinetic regimes	S^{mt}	S_{rx}	S_{rx} (low $[OH]_g$) S_{bd} (high $[OH]_g$)

concentration) is ~1, showing that bulk-to-surface transport of organics is sufficiently fast without kinetic limitation by bulk diffusion. In this case, the overall OH uptake is mainly limited by surface reaction (S_{rx}), and also partly by gas-phase diffusion as C_g is still ~0.3. In case of low $[OH]_g$ with <~10^8 cm^{-3}, SMP_Y stays at ~1 and γ_{OH} stays at ~0.1 over the entire simulation time.

At high OH concentration $[OH]_g \geq 10^9$ cm^{-3}, SMP_Y decreases to ~0.02, and γ_{OH} decreases substantially after ~1 s. In such a case, the surface reaction is limited by bulk diffusion of organics from the bulk to the surface (S_{bd}). At $[OH]_g = 5 \times 10^{10}$ cm^{-3}, the surface loss rate of levoglucosan is about 4 orders of magnitude higher than that at $[OH]_g = 5 \times 10^6$ cm^{-3}.

DOI: 10.1021/jp510489z
J. Phys. Chem. A 2015, 119, 4533−4544

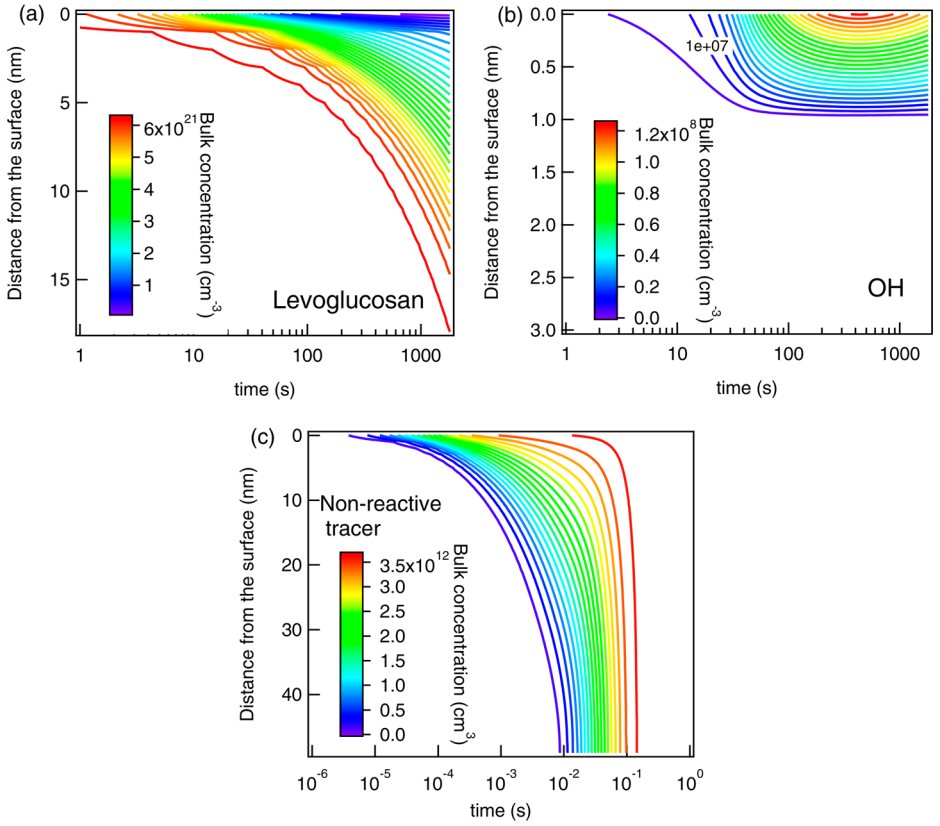

Figure 8. Evolution of the bulk concentration profile of (a) levoglucosan and (b) OH as a response to OH exposure of 5×10^{10} cm^{-3}. (c) Evolution of the bulk concentration profile of nonreactive tracer in the absence of chemical reactions but the same diffusivity as OH.

As the surface loss rate is larger than the diffusion flux of organics to the surface, levoglucosan at the surface is depleted followed by evaporation of volatile reaction products (e.g., glucic acid or 2-hydroxypropanedial).[29] Consequently, a strong concentration gradient of levoglucosan in the bulk develops after ~10 s, as shown in Figure 8a. Up to ~10 s, the bulk is free of OH radicals as most of them reacted away at the surface (Figure 8b). After ~10 s when levoglucosan is depleted at the surface, OH starts to diffuse into the near-surface bulk.

Note that constraining the reaction zone to the near-surface bulk is the result of the interplay between the diffusion and reaction of both levoglucosan and OH. The diffusivity of OH alone, neglecting reaction, would allow significant penetration into the bulk as demonstrated by the very fast incorporation into the bulk of an unreactive tracer with the same diffusion coefficient as OH (Figure 8c).

In summary, the temporal evolution of the limiting cases is depicted by arrows on the kinetic cube in Figure 6b: $S^{mt} \rightarrow S_{rx} \rightarrow S_{bd}$. For confirmation of the identified kinetic regimes and limiting cases and identification of the sensitive kinetic parameters, we conduct a sensitivity analysis by varying each kinetic parameter by 1 order of magnitude. Sensitivity of an input parameter λ_i on the modeled uptake coefficient, γ_{OH}, can be expressed through its normalized sensitivity coefficient $S^n(\lambda_i)$ defined as follows:[51]

$$S^n(\lambda_i) = \frac{\Delta \ln \gamma_{OH}}{\Delta \ln \lambda_i} \quad (1)$$

$S^n(\lambda_i)$ is derived by applying two different $[OH]_g$ (1×10^{10} cm^{-3} and 5×10^6 cm^{-3}) for the reaction time 0.01 and 1800 s: at 0.01 s the limiting case is expected to be S_{rx}; at 1800 s it is expected to be S_{rx} at low $[OH]_g$ and S_{bd} at high $[OH]_g$ (see Figure 4a).

Table 2 shows the results of such calculations. $S^n(\lambda_i)$ for k_{BR}, $K_{sol,cc}$, and D_{OH} are practically zero, indicating OH uptake is insensitive to these bulk-process-related parameters at both high and low $[OH]_g$. k_{SLR}, τ_d, and $\alpha_{s,0}$ are the most sensitive parameters, confirming that the OH uptake is dominated by surface processes. $S^n(k_{SLR})$ and $S^n(\tau_d)$ values are similar, showing that both parameters regulating surface reaction rates are equally important. At high OH concentrations in the S_{bd} region, $S^n(k_{SLR})$, $S^n(\tau_d)$, and $S^n(\alpha_{s,0})$ are about zero. γ_{OH} is sensitive to D_{org} only at high OH concentration and after a long

Table 2. Sensitivity Analysis Coefficient for Low $[OH]_g = 5 \times 10^6$ cm^{-3} and High $[OH]_g = 1 \times 10^{10}$ cm^{-3} Exposure Simulations[a]

	S^n							
	$[OH]_g = 5 \times 10^6$ cm^{-3}				$[OH]_g = 1 \times 10^{10}$ cm^{-3}			
	$t = 10^{-2}$ s		$t = 1.8 \times 10^3$ s		$t = 10^{-2}$ s		$t = 1.8 \times 10^3$ s	
	↑	↓	↑	↓	↑	↓	↑	↓
$\alpha_{s,0}$		1		1		1		0.01
τ_d	0.63	0.93	0.63	0.94	0.63	0.93	0	0.01
k_{slr}	0.63	0.94	0.63	0.94	0.63	0.93	0	0.01
k_{BR}	0	0	0	0	0	0	0	0
$K_{sol,cc}$	0	0	0	0	0	0	0	0
D_{OH}	0	0	0	0	0	0	0	0
D_{org}	0	0	0	0	0	0	0.49	0.50

[a] ↑ and ↓ denote an increase and a decrease of each parameter by 1 order of magnitude, respectively.

DOI: 10.1021/jp510489z
J. Phys. Chem. A 2015, 119, 4533−4544

exposure time, confirming that the OH uptake is limited by the bulk diffusivity of levoglucosan. OH uptake by abietic acid shows very similar sensitivity.

The reduction of γ_{OH} upon increase of gas-phase OH concentrations (Figures 2a and 3a) is a typical behavior of the so-called Langmuir−Hinshelwood mechanism, in which an adsorbed molecule reacts with organics by surface reaction. This is in contrast to the Eley−Rideal mechanism, in which a single kinetic step of collision and reaction occurs between gaseous species and surface molecules.[49] OH has been considered to undergo Eley−Rideal mechanism due to its high reactivity, but our findings are consistent with recent studies[29,41,74−76] suggesting that OH follows Langmuir−Hinshelwood behavior. Reduction of γ_{OH} at high gas-phase concentration is associated with saturation of gaseous species at the surface, which is caused by relatively slower surface reaction rates in the case of less reactive gas species such as ozone.[48,77,78] In the case of OH, accumulation at the surface (e.g., SSR ≈ 1; see Figure 7) is due to reduced surface reaction rates limited by bulk diffusion of levoglucosan or abietic acid.

■ ATMOSPHERIC IMPLICATION

We estimate the chemical half-life, $t_{1/2}$, of levoglucosan and abietic acid by multiphase chemical reactions of OH radicals for a range of ambient RH and temperature. $t_{1/2}$ is defined as the time after which the number of organic molecules in the condensed phase has decreased to half of its initial value. We consider a pure levoglucosan or abietic acid particle with a diameter of 200 nm. $t_{1/2}$ for abietic acid is found to be ∼30% longer than that for levoglucosan, and we focus our analysis on levoglucosan. $[OH]_g$ ranges from 10^6 cm^{-3} in typical pristine environments to ∼10^8 cm^{-3} in the fresh biomass burning plumes.[5] We consider two scenarios representing dry conditions and cloud processing occurring in the boundary layer at 25 °C. At dry conditions, the same kinetic parameters set for the simulations reported in Figure 2 are used. Under high RH, levoglucosan undergoes a moisture-induced phase transition transforming from an amorphous semisolid to a liquid phase.[65] For the cloud processing scenario, bulk diffusion coefficients of OH and levoglucosan are increased to 10^{-5} and 10^{-7} cm^2 s^{-1}, respectively, and the Henry's law coefficient of OH in water is used (2.5×10^{-2} mol cm^{-3} atm^{-1}).[71] $k_{BR} = 1.8 \times 10^{-12}$ cm^3 s^{-1} is used as reported by Zhao et al.[28] Other parameters are kept the same as for dry conditions to explore and characterize the effects of bulk diffusion and OH solubility on the multiphase reactions of BBA.

Biomass burning is often associated with strong convection, and the plume can reach the midtroposphere and possibly also upper troposphere and lower stratosphere.[6−8,79] We simulate $t_{1/2}$ under lower temperatures of 10 and 0 °C. The glass transition temperature (T_g) of levoglucosan is determined to be ∼283 ± 17 K,[67] at which levoglucosan undergoes glass transition with a viscosity exceeding ∼10^{12} Pa s, corresponding to bulk diffusivity (D_{LG}) < ∼10^{-20} cm^2 s^{-1} based on the Stokes−Einstein relation. A recent study shows that the Stokes−Einstein relation may break down close to T_g.[80] We assume that $D_{LG} = 10^{-18}$ cm^2 s^{-1} at 10 °C and 10^{-20} cm^2 s^{-1} below 0 °C. The temperature dependence of bulk diffusivity of H_2O in levoglucosan can be estimated using a semiempirical parametrization developed by Berkemeier et al.[81] based on a Vogel−Fulcher−Tammann approach. Figure 9 shows the estimated D_w with uncertainty reflecting the uncertainty of the input parameter T_g. Considering D_{OH} should be slightly larger than D_w, we use the upper estimate of D_w for calculations. $t_{1/2}$ at 10 and below 0 °C are simulated using the estimated bulk diffusivity and keeping all other parameters the same. Note that a decrease of the reaction rate coefficients with decreasing temperature may increase $t_{1/2}$ further; thus our estimates can be regarded as lower limits.

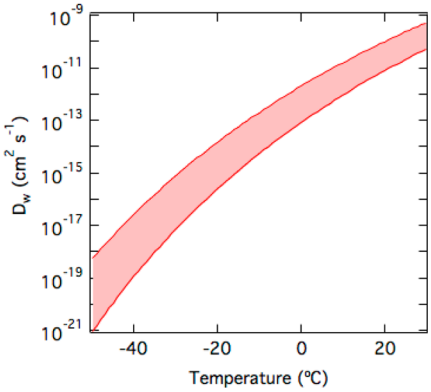

Figure 9. Diffusion coefficient of H_2O as a function of temperature estimated using a parametrization[81] based on a Vogel−Fulcher−Tammann approach.

Figure 10a shows $t_{1/2}$ for levoglucosan simulated as a function of gas-phase OH concentration for different temperatures and humidity. At dry conditions $t_{1/2}$ is more than 37 days for $[OH]_g$ of ∼3×10^6 cm^{-3} and $t_{1/2}$ decreases to more than 1 week for biomass burning plume conditions with $[OH]_g > 10^7$ cm^{-3}. Under cloud processing conditions at 25 °C, $t_{1/2}$ is ∼9 days at $[OH]_g \sim 3 \times 10^6$ cm^{-3} and less than 3 days in a biomass burning plume with $[OH]_g > 10^7$ cm^{-3}, due to the absence of kinetic limitations of mass transport in the particle phase with the high bulk diffusivity of levoglucosan and OH and high OH water solubility. At low temperatures $t_{1/2}$ increases substantially to about 1 month at 10 °C and can be over a year below 0 °C. Below T_g, $t_{1/2}$ stays almost constant as levoglucosan is practically degraded only at the surface and levoglucosan in the bulk is shielded well in a glassy matrix.

This behavior is consistent with the results of previous studies reporting the importance of the particle phase state for the chemical aging of aerosols.[35,37,59,82] For levoglucosan films, Lai et al.[33] observed a decrease of reactivity upon increase of relative humidity which may be a consequence of the blocking surface reactive sites by adsorbed water molecules.[35,65] The estimated chemical half-life is comparable with previously reported *e*-folding time of levoglucosan under dry and humid conditions[29,31,35] and in aqueous solution,[28,32,34] ranging from 1 day to more than a month depending on ambient relative humidity and gas-phase OH concentration.

Levoglucosan is widely used as a molecular marker of biomass burning in source apportionment studies with the assumption that the marker is stable up to 1 week during its transportation in the atmosphere.[22,83] Figure 10b shows the degraded fraction of levoglucosan contained in a 200 nm diameter particle upon exposure to a range of OH concentrations for 1 week under cloud processing and dry conditions at 10 and 0 °C. The calculations indicate that 12% of levoglucosan is degraded under ambient OH concentrations of 3×10^6 cm^{-3} under dry conditions at 25 °C. The degraded fraction reaches more than 40% under cloud processing. If the plume stays in the boundary layer and lower troposphere, about 30−50% of levoglucosan may be degraded after 1 week of OH

DOI: 10.1021/jp510489z
J. Phys. Chem. A 2015, 119, 4533−4544

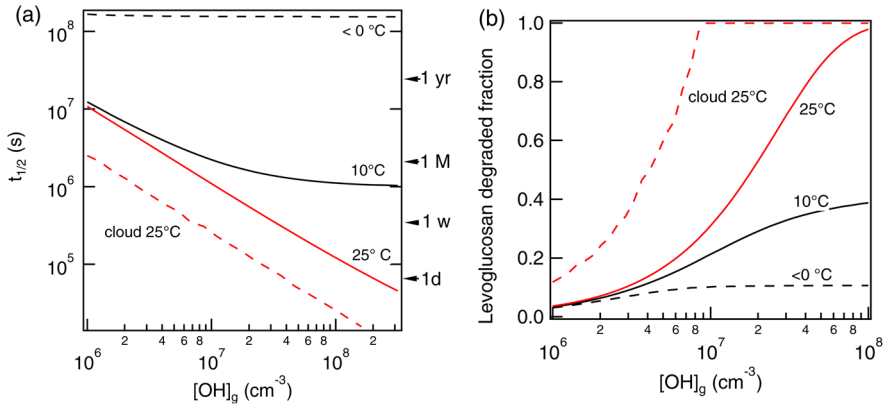

Figure 10. (a) Chemical half-life of levoglucosan in a particle with 200 nm diameter for different environmental conditions: at 25 °C under dry (solid red line) and cloud conditions (dashed red line), and at 10 °C (solid black line) and below 0 °C (dashed black line) under dry conditions. (b) Degraded fraction of levoglucosan after 1 week exposure at different OH concentrations at 25 °C under dry (solid red line) and cloud conditions (dashed red line), and at 10 °C (solid black line) and below 0 °C (dashed black line) under dry conditions.

exposure. Most of levoglucosan may be depleted particularly under high OH concentrations and humid conditions. In the case of strong plume convection reaching higher altitudes and thus lower temperatures, up to ∼30% and ∼10% of levoglucosan may be degraded at 10 and 0 °C, respectively. This estimation is consistent with aircraft observations, finding a large amount of biomass burning aerosol even in the highly aged plumes in the midtroposphere and upper troposphere.[8,79,84]

Note that levoglucosan and abietic acid are reactive toward other oxidants such as O_3 and NO_3.[36,37,85] Moreover, they are semivolatile and partition to the gas phase, where it can be degraded by gas-phase reactions with various oxidants.[86−88] BBAs consist of a mixture of organic and inorganic compounds possibly multiphase in nature,[83,89] potentially shielding organics from oxidants thereby impacting the degradation kinetics as has been shown previously in the case of O_3 oxidation.[90−92] For comprehensive understanding of chemical aging of biomass burning markers, partitioning and gas-phase and multiphase oxidation should be accounted for in models.[93−96] For the reasons listed previously, the chemical half-life estimated in this work is considered as an upper limit. Nevertheless, the simulation results suggest that the air mass history (RH and temperature) play a crucial role in source apportionment studies applying levoglucosan and abietic acid as molecular markers. Aerosol apportionment studies may account for degradation of these markers using estimates derived here and apply additional markers, such as, e.g., CH_3CN,[97] to improve prediction of aerosol source strengths.

CONCLUSION

We have applied the kinetic multilayer model to coated-wall flow-tube experiments for OH exposure to levoglucosan and abietic acid, which serve as surrogates and molecular markers of biomass burning aerosols. The bulk diffusion coefficient of OH in the organic material is estimated to be $\sim 10^{-10}$ cm^2 s^{-1}, and diffusivity of levoglucosan and abietic acid to be $\sim 10^{-16}$ cm^2 s^{-1}, characteristic of an amorphous semisolid state. The sensitivity studies reveal that OH uptake is dominated by surface reactions at ambient relevant OH concentrations ($<10^7$ cm^{-3}) but can be limited by the surface-bulk exchange and bulk diffusion upon increase of OH gas-phase concentration. We assessed that it can take 1 week to degrade 50% of the molecules contained in 200 nm sized particles by OH under dry conditions, while it takes only several days upon liquefaction under cloud processing. If a biomass burning plume is transported to the midtroposphere or upper troposphere by convection, the chemical half-life of the organic compounds can be more than a month due to slow bulk diffusion as a consequence of low temperatures. The findings demonstrate that multiphase chemical aging of condensed-phase organic material by OH depends strongly on environmental conditions such as RH and temperature. This has important implications for source apportionment studies but also for the evolution of organic aerosol in the atmosphere in general, and as such for aerosol radiative properties and aerosol cloud formation potential.

Though this study is unique in its kind and allows for a much improved fundamental understanding of the underlying molecular processes governing the OH reactive uptake and multiphase kinetics, it is not complete and many points still have to be addressed in future studies to better resolve the involved mechanisms and to yield a more accurate prediction of the atmospheric evolution of organic aerosol. From this combined experimental and modeling study, we can conclude and suggest the following key points that warrant further investigation into the nature of multiphase kinetics.

1. Temperature and RH Effect. The troposphere experiences large variations in temperature and RH. Most of the troposphere exhibits temperatures lower than 273 K, i.e., much lower than temperatures typically applied in experimental kinetics studies involving organic aerosol. Also, RH varies significantly within the troposphere from a few percent to saturation in clouds. Organic aerosols exhibit various phase states (liquid, semisolid, or amorphous solid) depending on temperature and RH, undergoing moisture-induced or temperature-induced glass transition.[98] Clearly, this has subsequent effects on the multiphase kinetics of atmospheric trace gases due to changes in oxidant and organics diffusivity.[35,59,82,92,99,100] Frozen or solid organic substrates typically exhibit a much lower uptake than their liquid counterparts.[39,91,101,102] Moreover, multicomponent mixtures of inorganic and organic species can undergo liquid−liquid phase transition in response to changes in RH.[103−105] These complex processes result in a wide range of multiphase kinetics for varying temperature and RH for the same particle system. These processes not only impact the chemical aging of organic aerosol but also formation

DOI: 10.1021/jp510489z
J. Phys. Chem. A 2015, 119, 4533−4544

and partitioning of SOA[60,106] and cloud formation potential.[43,81,107]

2. Volatilization and Subsequent Gas-Phase Chemistry. OH oxidation of organic substrates can lead to volatilization.[29,57,108,109] Volatilized products can further react with OH in the gas phase, providing an additional sink for OH, making kinetics simulations of flow tube and chamber experiments more challenging. This may also be crucial for estimates of the atmospheric OH budget in a biomass burning plume. Gas-phase reactions may yield semivolatile and low-volatile oxidation products that can recondense on particulate matter.[40] Experiments should aim to measure gas-phase composition during kinetic experiments to place upper/lower limits on the contribution of gas-phase reaction kinetics to overall OH loss. The kinetic flux model[50] as applied here can be a useful tool to investigate such aspects.

3. Interplay of Gas Uptake and Bulk Diffusion. This study indicates that diffusion of substrate molecules can play a crucial role in the overall uptake kinetics even for an amorphous semisolid organic substrate. Substrate diffusion was also found to be important in ozonolysis of polycyclic aromatic hydrocarbons coated by amorphous semisolid SOA coatings.[100] Diffusion processes in the bulk can occur in parallel to surface reaction and reversible adsorption. In this study we have demonstrated different dominating regimes depending on OH gas-phase concentration for which the uptake can be limited by surface reaction or by bulk-to-surface transport, the latter being strongly dependent on substrate diffusivity. It can be expected that these regimes will vary in response to changes in organic phase state due to changes in RH and temperature making prediction of these multiphase chemical kinetics involving atmospheric organic aerosol even more complicated. Our findings challenge the application of simple Langmuir–Hinshelwood and Eley–Rideal mechanisms to organic substrates. Novel experimental approaches that can deconvolute surface processes from bulk processes or application of combined experimental and modeling techniques are necessary to improve our understanding of the chemical aging processes of organic aerosols.

AUTHOR INFORMATION

Corresponding Authors

*(M.S.) E-mail: m.shiraiwa@mpic.de.

*(D.A.K.) E-mail: daniel.knopf@stonybrook.edu.

Notes

The authors declare no competing financial interest.

ACKNOWLEDGMENTS

We thank two anonymous reviewers for useful comments. A.M.A., T.B., U.P., and M.S. acknowledge support by the Pan-European Gas-AeroSOls-climate interaction Study (No. 265148, PEGASOS). J.H.S. and D.A.K. acknowledge support by the National Science Foundation, Grant AGS-0846255. T. B. was supported by the Max Planck Graduate Center with the Johannes Gutenberg-Universität Mainz (MPGC).

REFERENCES

(1) Bond, T. C.; Doherty, S. J.; Fahey, D. W.; Forster, P. M.; Berntsen, T.; DeAngelo, B. J.; Flanner, M. G.; Ghan, S.; Karcher, B.; Koch, D.; Kinne, S.; Kondo, Y.; Quinn, P. K.; Sarofim, M. C.; Schultz, M. G.; Schulz, M.; Venkataraman, C.; Zhang, H.; Zhang, S.; Bellouin, N.; Guttikunda, S. K.; Hopke, P. K.; Jacobson, M. Z.; Kaiser, J. W.; Klimont, Z.; Lohmann, U.; Schwarz, J. P.; Shindell, D.; Storelvmo, T.; Warren, S. G.; Zender, C. S. Bounding the role of black carbon in the climate system: A scientific assessment. *J. Geophys. Res.: Atmos.* **2013**, *118* (11), 5380–5552.

(2) Crutzen, P. J.; Andreae, M. O. Biomass burning in the tropics: Impact on atmospheric chemistry and biogeochemical cycles. *Science* **1990**, *250* (4988), 1669–1678.

(3) Andreae, M. O.; Merlet, P. Emission of trace gases and aerosols from biomass burning. *Global Biogeochem. Cycles* **2001**, *15* (4), 955–966.

(4) Janhäll, S.; Andreae, M. O.; Pöschl, U. Biomass burning aerosol emissions from vegetation fires: Particle number and mass emission factors and size distributions. *Atmos. Chem. Phys.* **2010**, *10*, 1427–1439.

(5) Hobbs, P. V.; Sinha, P.; Yokelson, R. J.; Christian, T. J.; Blake, D. R.; Gao, S.; Kirchstetter, T. W.; Novakov, T.; Pilewskie, P. Evolution of gases and particles from a savanna fire in South Africa. *J. Geophys. Res.: Atmos.* **2003**, *108* (D13), No. 8485.

(6) Jost, H. J.; Drdla, K.; Stohl, A.; Pfister, L.; Loewenstein, M.; Lopez, J. P.; Hudson, P. K.; Murphy, D. M.; Cziczo, D. J.; Fromm, M.; Bui, T. P.; Dean-Day, J.; Gerbig, C.; Mahoney, M. J.; Richard, E. C.; Spichtinger, N.; Pittman, J. V.; Weinstock, E. M.; Wilson, J. C.; Xueref, I. In-situ observations of mid-latitude forest fire plumes deep in the stratosphere. *Geophys. Res. Lett.* **2004**, *31* (11), No. L11101.

(7) Fromm, M.; Lindsey, D. T.; Servranckx, R.; Yue, G.; Trickl, T.; Sica, R.; Doucet, P.; Godin-Beekmann, S. E. The Untold Story of Pyrocumulonimbus. *Bull. Am. Meteorol. Soc.* **2010**, *91* (9), 1193–1209.

(8) Hudson, P. K.; Murphy, D. M.; Cziczo, D. J.; Thomson, D. S.; de Gouw, J. A.; Warneke, C.; Holloway, J.; Jost, J. R.; Hubler, G. Biomass-burning particle measurements: Characteristic composition and chemical processing. *J. Geophys. Res.: Atmos.* **2004**, *109* (D23), No. D23S27.

(9) Andreae, M. O.; Rosenfeld, D.; Artaxo, P.; Costa, A. A.; Frank, G. P.; Longo, K. M.; Silva-Dias, M. A. F. Smoking rain clouds over the Amazon. *Science* **2004**, *303* (5662), 1337–1342.

(10) Vakkari, V.; Kerminen, V. M.; Beukes, J. P.; Tiitta, P.; van Zyl, P. G.; Josipovic, M.; Venter, A. D.; Jaars, K.; Worsnop, D. R.; Kulmala, M.; Laakso, L. Rapid changes in biomass burning aerosols by atmospheric oxidation. *Geophys. Res. Lett.* **2014**, *41* (7), 2644–2651.

(11) Shantz, N. C.; Gultepe, I.; Andrews, E.; Zelenyuk, A.; Earle, M. E.; Macdonald, A. M.; Liu, P. S. K.; Leaitch, W. R. Optical, physical, and chemical properties of springtime aerosol over Barrow Alaska in 2008. *Int. J. Climatol.* **2014**, *34* (10), 3125–3138.

(12) Stocker, T. F., Qin, D., Plattner, G.-K., Tignor, M., Allen, S. K., Boschung, J., Nauels, A., Xia, Y., Bex, V., Midgley, P. M., Eds. *Climate change 2013: The physical science basis*, Working Group I Contribution to the Fifth IPCC Assessment Report; Intergovernmental Panel on Climate Change: Bern, Switzerland, 2013.

(13) Ramanathan, V.; Carmichael, G. Global and regional climate changes due to black carbon. *Nat. Geosci.* **2008**, *1* (4), 221–227.

(14) de Oliveira Alves, N.; Matos Loureiro, A. L.; Dos Santos, F. C.; Nascimento, K. H.; Dallacort, R.; de Castro Vasconcellos, P.; de Souza Hacon, S.; Artaxo, P.; de Medeiros, S. R. Genotoxicity and composition of particulate matter from biomass burning in the eastern Brazilian Amazon region. *Ecotoxicol. Environ. Saf.* **2011**, *74* (5), 1427–33.

(15) de Oliveira Alves, N.; de Souza Hacon, S.; de Oliveira Galvao, M. F.; Simoes Peixotoc, M.; Artaxo, P.; de Castro Vasconcellos, P.; de Medeiros, S. R. Genetic damage of organic matter in the Brazilian Amazon: A comparative study between intense and moderate biomass burning. *Environ. Res.* **2014**, *130*, 51–58.

(16) Shiraiwa, M.; Selzle, K.; Pöschl, U. Hazardous components and health effects of atmospheric aerosol particles: Reactive oxygen species, soot, polycyclic aromatic compounds and allergenic proteins. *Free Radical Res.* **2012**, *46* (8), 927–939.

(17) Okoshi, R.; Rasheed, A.; Reddy, G. C.; McCrowey, C. J.; Curtis, D. B. Size and mass distributions of ground-level sub-micrometer biomass burning aerosol from small wildfires. *Atmos. Environ.* **2014**, *89*, 392–402.

DOI: 10.1021/jp510489z
J. Phys. Chem. A 2015, 119, 4533–4544

(18) Ichoku, C.; Kahn, R.; Chin, M. Satellite contributions to the quantitative characterization of biomass burning for climate modeling. *Atmos. Res.* **2012**, *111*, 1−28.
(19) Sang, X.; Zhang, Z.; Chan, C.; Engling, G. Source categories and contribution of biomass smoke to organic aerosol over the southeastern Tibetan Plateau. *Atmos. Environ.* **2013**, *78*, 113−123.
(20) Viana, M.; Reche, C.; Amato, F.; Alastuey, A.; Querol, X.; Moreno, T.; Lucarelli, F.; Nava, S.; Calzolai, G.; Chiari, M.; Rico, M. Evidence of biomass burning aerosols in the Barcelona urban environment during winter time. *Atmos. Environ.* **2013**, *72*, 81−88.
(21) Capes, G.; Johnson, B.; McFiggans, G.; Williams, P. I.; Haywood, J.; Coe, H. Aging of biomass burning aerosols over West Africa: Aircraft measurements of chemical composition, microphysical properties, and emission ratios. *J. Geophys. Res.* **2008**, *113*, No. D00C15.
(22) Robinson, A. L.; Subramanian, R.; Donahue, N. M.; Bernardo-Bricker, A.; Rogge, W. F. Source apportionment of molecular markers and organic aerosol. 2. Biomass smoke. *Environ. Sci. Technol.* **2006**, *40* (24), 7811−7819.
(23) Simoneit, B. R. T.; Schauer, J. J.; Nolte, C. G.; Oros, D. R.; Elias, V. O.; Fraser, M. P.; Rogge, W. F.; Cass, G. R. Levoglucosan, a tracer for cellulose in biomass burning and atmospheric particles. *Atmos. Environ.* **1999**, *33*, 173−182.
(24) Fraser, M. P.; Lakshmanan, K. Using levoglucosan as a molecular marker for the long-range transport of biomass combustion aerosols. *Environ. Sci. Technol.* **2000**, *34* (21), 4560−4564.
(25) Hu, Q. H.; Xie, Z. Q.; Wang, X. M.; Kang, H.; Zhang, P. Levoglucosan indicates high levels of biomass burning aerosols over oceans from the Arctic to Antarctic. *Sci. Rep.* **2013**, *3*, No. 3119.
(26) Mochida, M.; Kawamura, K.; Fu, P. Q.; Takemura, T. Seasonal variation of levoglucosan in aerosols over the western North Pacific and its assessment as a biomass-burning tracer. *Atmos. Environ.* **2010**, *44* (29), 3511−3518.
(27) Saarikoski, S.; Timonen, H.; Saarnio, K.; Aurela, M.; Järvi, L.; Keronen, P.; Kerminen, V. M.; Hillamo, R. Sources of organic carbon in fine particulate matter in northern European urban air. *Atmos. Chem. Phys.* **2008**, *8* (20), 6281−6295.
(28) Zhao, R.; Mungall, E. L.; Lee, A. K. Y.; Aljawhary, D.; Abbatt, J. P. D. Aqueous-phase photooxidation of levoglucosan—A mechanistic study using aerosol time of flight chemical ionization mass spectrometry (Aerosol-ToF-CIMS). *Atmos. Chem. Phys.* **2014**, *14*, 9695−9706.
(29) Slade, J. H.; Knopf, D. A. Heterogeneous OH oxidation of biomass burning organic aerosol surrogate compounds: Assessment of volatilisation products and the role of OH concentration on the reactive uptake kinetics. *Phys. Chem. Chem. Phys.* **2013**, *15* (16), 5898−5915.
(30) Hennigan, C. J.; Sullivan, A. P.; Collett, J. L.; Robinson, A. L. Levoglucosan stability in biomass burning particles exposed to hydroxyl radicals. *Geophys. Res. Lett.* **2010**, *37*, No. L09806.
(31) Kessler, S. H.; Smith, J. D.; Che, D. L.; Worsnop, D. R.; Wilson, K. R.; Kroll, J. H. Chemical sinks of organic aerosol: Kinetics and products of the heterogeneous oxidation of erythritol and levoglucosan. *Environ. Sci. Technol.* **2010**, *44* (18), 7005−10.
(32) Hoffmann, D.; T, A.; Iinuma, Y.; Herrmann, H. Atmospheric Stability of Levoglucosan: A Detailed Laboratory and Modeling Study. *Environ. Sci. Technol.* **2010**, *44* (2), 694−699.
(33) Lai, C.; Liu, Y.; Ma, J.; Ma, Q.; He, H. Degradation kinetics of levoglucosan initiated by hydroxyl radical under different environmental conditions. *Atmos. Environ.* **2014**, *91*, 32−39.
(34) Teraji, T.; Arakaki, T. Bimolecular Rate Constants between Levoglucosan and Hydroxyl Radical: Effects of pH and Temperature. *Chem. Lett.* **2010**, *39* (8), 900−901.
(35) Slade, J. H.; Knopf, D. A. Multiphase OH oxidation kinetics of organic aerosol: The role of particle phase state and relative humidity. *Geophys. Res. Lett.* **2014**, *41* (14), 5297−5306.
(36) Knopf, D. A.; Forrester, S. M.; Slade, J. H. Heterogeneous oxidation kinetics of organic biomass burning aerosol surrogates by O_3, NO_2, N_2O_5, and NO_3. *Phys. Chem. Chem. Phys.* **2011**, *13* (47), 21050−21062.
(37) Shiraiwa, M.; Pöschl, U.; Knopf, D. A. Multiphase chemical kinetics of NO_3 radicals reacting with organic aerosol components from biomass burning. *Environ. Sci. Technol.* **2012**, *46* (12), 6630−6636.
(38) Pöschl, U. Atmospheric aerosols: Composition, transformation, climate and health effects. *Angew. Chem., Int. Ed.* **2005**, *44* (46), 7520−7540.
(39) Rudich, Y.; Donahue, N. M.; Mentel, T. F. Aging of organic aerosol: Bridging the gap between laboratory and field studies. *Annu. Rev. Phys. Chem.* **2007**, *58*, 321−352.
(40) Jimenez, J. L.; Canagaratna, M. R.; Donahue, N. M.; Prevot, A. S.; Zhang, Q.; Kroll, J. H.; DeCarlo, P. F.; Allan, J. D.; Coe, H.; Ng, N. L.; Aiken, A. C.; Docherty, K. S.; Ulbrich, I. M.; Grieshop, A. P.; Robinson, A. L.; Duplissy, J.; Smith, J. D.; Wilson, K. R.; Lanz, V. A.; Hueglin, C.; Sun, Y. L.; Tian, J.; Laaksonen, A.; Raatikainen, T.; Rautiainen, J.; Vaattovaara, P.; Ehn, M.; Kulmala, M.; Tomlinson, J. M.; Collins, D. R.; Cubison, M. J.; Dunlea, E. J.; Huffman, J. A.; Onasch, T. B.; Alfarra, M. R.; Williams, P. I.; Bower, K.; Kondo, Y.; Schneider, J.; Drewnick, F.; Borrmann, S.; Weimer, S.; Demerjian, K.; Salcedo, D.; Cottrell, L.; Griffin, R.; Takami, A.; Miyoshi, T.; Hatakeyama, S.; Shimono, A.; Sun, J. Y.; Zhang, Y. M.; Dzepina, K.; Kimmel, J. R.; Sueper, D.; Jayne, J. T.; Herndon, S. C.; Trimborn, A. M.; Williams, L. R.; Wood, E. C.; Middlebrook, A. M.; Kolb, C. E.; Baltensperger, U.; Worsnop, D. R. Evolution of organic aerosols in the atmosphere. *Science* **2009**, *326* (5959), 1525−9.
(41) George, I. J.; Abbatt, J. P. Heterogeneous oxidation of atmospheric aerosol particles by gas-phase radicals. *Nat. Chem.* **2010**, *2* (9), 713−722.
(42) Petters, M. D.; Prenni, A. J.; Kreidenweis, S. M.; DeMott, P. J.; Matsunaga, A.; Lim, Y. B.; Ziemann, P. J. Chemical aging and the hydrophobic-to-hydrophilic conversion of carbonaceous aerosol. *Geophys. Res. Lett.* **2006**, *33* (24), No. L24806.
(43) Wang, B.; Knopf, D. A. Heterogeneous ice nucleation on particles composed of humic-like substances impacted by O_3. *J. Geophys. Res.* **2011**, *116* (D3), No. D03205.
(44) Wang, B. B.; Laskin, A.; Roedel, T.; Gilles, M. K.; Moffet, R. C.; Tivanski, A. V.; Knopf, D. A. Heterogeneous ice nucleation and water uptake by field-collected atmospheric particles below 273 K. *J. Geophys. Res.: Atmos.* **2012**, *117* (D21), No. D00V19.
(45) Zhang, X.; Lin, Y. H.; Surratt, J. D.; Weber, R. J. Sources, composition and absorption Angstrom exponent of light-absorbing organic components in aerosol extracts from the Los Angeles Basin. *Environ. Sci. Technol.* **2013**, *47* (8), 3685−3693.
(46) Flores, J. M.; Washenfelder, R. A.; Adler, G.; Lee, H. J.; Segev, L.; Laskin, J.; Laskin, A.; Nizkorodov, S. A.; Brown, S. S.; Rudich, Y. Complex refractive indices in the near-ultraviolet spectral region of biogenic secondary organic aerosol aged with ammonia. *Phys. Chem. Chem. Phys.* **2014**, *16* (22), 10629−10642.
(47) Liu, J.; Scheuer, E.; Dibb, J.; Ziemba, L. D.; Thornhill, K. L.; Anderson, B. E.; Wisthaler, A.; Mikoviny, T.; Devi, J. J.; Bergin, M.; Weber, R. J. Brown carbon in the continental troposphere. *Geophys. Res. Lett.* **2014**, *41* (6), 2191−2195.
(48) Shiraiwa, M.; Sosedova, Y.; Rouviere, A.; Yang, H.; Zhang, Y.; Abbatt, J. P.; Ammann, M.; Pöschl, U. The role of long-lived reactive oxygen intermediates in the reaction of ozone with aerosol particles. *Nat. Chem.* **2011**, *3* (4), 291−295.
(49) Pöschl, U.; Rudich, Y.; Ammann, M. Kinetic model framework for aerosol and cloud surface chemistry and gas-particle interactions—Part 1: General equations, parameters, and terminology. *Atmos. Chem. Phys.* **2007**, *7*, 5989−6023.
(50) Shiraiwa, M.; Pfrang, C.; Koop, T.; Pöschl, U. Kinetic multi-layer model of gas-particle interactions in aerosols and clouds (KM-GAP): Linking condensation, evaporation and chemical reactions of organics, oxidants and water. *Atmos. Chem. Phys.* **2012**, *12* (5), 2777−2794.
(51) Berkemeier, T.; Huisman, A. J.; Ammann, M.; Shiraiwa, M.; Koop, T.; Pöschl, U. Kinetic regimes and limiting cases of gas uptake

DOI: 10.1021/jp510489z
J. Phys. Chem. A 2015, 119, 4533−4544

and heterogeneous reactions in atmospheric aerosols and clouds: A general classification scheme. *Atmos. Chem. Phys.* **2013**, *13* (14), 6663−6686.
(52) Shiraiwa, M.; Berkemeier, T.; Schilling-Fahnestock, K. A.; Seinfeld, J. H.; Pöschl, U. Molecular corridors and kinetic regimes in the multiphase chemical evolution of secondary organic aerosol. *Atmos. Chem. Phys.* **2014**, *14* (16), 8323−8341.
(53) Knopf, D. A.; Pöschl, U.; Shiraiwa, M. Flow and Flux-Based Analytical Solution of Gas-Phase Diffusion Correction for Tubular Flow Reactors with an Absorbing or Reactive Wall Surface. *Anal. Chem.*, **2015**, under review.
(54) Brown, R. L. Tubolar Flow Reactors with First-Order Kinetics. *J. Res. Natl. Bur. Stand.* **1978**, *83* (1), 1−8.
(55) Bai, J.; Sun, X.; Zhang, C.; Xu, Y.; Qi, C. The OH-initiated atmospheric reaction mechanism and kinetics for levoglucosan emitted in biomass burning. *Chemosphere* **2013**, *93* (9), 2004−2010.
(56) Houle, F. A.; Hinsberg, W. D.; Wilson, K. R. Oxidation of a model alkane aerosol by OH radical: The emergent nature of reactive uptake. *Phys. Chem. Chem. Phys.* **2015**, *17* (6), 4412−4423.
(57) Bertram, A. K.; Ivanov, A. V.; Hunter, M.; Molina, L. T.; Molina, M. J. The reaction probability of OH on organic surfaces of tropospheric interest. *J. Phys. Chem. A* **2001**, *105* (41), 9415−9421.
(58) Vieceli, J.; Roeselova, M.; Potter, N.; Dang, L. X.; Garrett, B. C.; Tobias, D. J. Molecular dynamics simulations of atmospheric oxidants at the air-water interface: Solvation and accommodation of OH and O_3. *J. Phys. Chem. B* **2005**, *109* (33), 15876−15892.
(59) Shiraiwa, M.; Ammann, M.; Koop, T.; Pöschl, U. Gas uptake and chemical aging of semisolid organic aerosol particles. *Proc. Natl. Acad. Sci. U. S. A.* **2011**, *108* (27), 11003−11008.
(60) Shiraiwa, M.; Yee, L. D.; Schilling, K. A.; Loza, C. L.; Craven, J. S.; Zuend, A.; Ziemann, P. J.; Seinfeld, J. H. Size distribution dynamics reveal particle-phase chemistry in organic aerosol formation. *Proc. Natl. Acad. Sci. U. S. A.* **2013**, *110* (29), 11746−11750.
(61) Atkins, P. W. *Physical Chemistry*; Oxford University Press: Oxford, U.K., 1998.
(62) Mak, C. H.; Brand, J. L.; Koehler, B. G.; George, S. M. Coverage dependence of the surface diffusion coefficient for hydrogen on Ru (001). *Surf. Sci.* **1987**, *191* (1), 108−120.
(63) Seebauer, E. G.; Allen, C. E. Estimating surface diffusion coefficients. *Prog. Surf. Sci.* **1995**, *49* (3), 265−330.
(64) Yokelson, R. J.; Crounse, J. D.; DeCarlo, P. F.; Karl, T.; Urbanski, S.; Atlas, E.; Campos, T.; Shinozuka, Y.; Kapustin, V.; Clarke, A. D.; Weinheimer, A.; Knapp, D. J.; Montzka, D. D.; Holloway, J.; Weibring, P.; Flocke, F.; Zheng, W.; Toohey, D.; Wennberg, P. O.; Wiedinmyer, C.; Mauldin, L.; Fried, A.; Richter, D.; Walega, J.; Jimenez, J. L.; Adachi, K.; Buseck, P. R.; Hall, S. R.; Shetter, R. Emissions from biomass burning in the Yucatan. *Atmos. Chem. Phys.* **2009**, *9* (15), 5785−5812.
(65) Mikhailov, E.; Vlasenko, S.; Martin, S. T.; Koop, T.; Pöschl, U. Amorphous and crystalline aerosol particles interacting with water vapor: Conceptual framework and experimental evidence for restructuring, phase transitions and kinetic limitations. *Atmos. Chem. Phys.* **2009**, *9*, 9491−9522.
(66) Price, H. C.; Murray, B. J.; Mattsson, J.; O'Sullivan, D.; Wilson, T. W.; Baustian, K. J.; Benning, L. G. Quantifying water diffusion in high-viscosity and glassy aqueous solutions using a Raman isotope tracer method. *Atmos. Chem. Phys.* **2014**, *14* (8), 3817−3830.
(67) Zobrist, B.; Marcolli, C.; Pedernera, D. A.; Koop, T. Do atmospheric aerosols form glasses? *Atmos. Chem. Phys.* **2008**, *8* (17), 5221−5244.
(68) Ediger, M. D.; Forrest, J. A. Dynamics near Free Surfaces and the Glass Transition in Thin Polymer Films: A View to the Future. *Macromolecules* **2014**, *47* (2), 471−478.
(69) Ivanov, A. V.; Trakhtenberg, S.; Bertram, A. K.; Gershenzon, Y. M.; Molina, M. J. OH, HO_2, and ozone gaseous diffusion coefficients. *J. Phys. Chem. A* **2007**, *111* (9), 1632−1637.
(70) Hanson, D. R.; Burkholder, J. B.; Howard, C. J.; Ravishankara, A. R. Measurement of hydroxyl and hydroperoxy radical uptake coefficients on water and sulfuric acid surfaces. *J. Phys. Chem.* **1992**, *96* (12), 4979−4985.
(71) Lelieveld, J.; Crutzen, P. J. The role of clouds in tropospheric photochemistry. *J. Atmos. Chem.* **1991**, *12* (3), 229−267.
(72) Jacob, D. J. Chemistry of OH in Remote Clouds and Its Role in the Production of Formic-Acid and Peroxymonosulfate. *J. Geophys. Res.: Atmos.* **1986**, *91* (D9), 9807−9826.
(73) Wiegel, A. A.; Wilson, K. R.; Hinsberg, W. D.; Houle, F. A. Stochastic methods for aerosol chemistry: A compact molecular description of functionalization and fragmentation in the heterogeneous oxidation of squalane aerosol by OH radicals. *Phys. Chem. Chem. Phys.* **2015**, *17* (6), 4398−4411.
(74) Enami, S.; Hoffmann, M. R.; Colussi, A. J. In situ mass spectrometric detection of interfacial intermediates in the oxidation of RCOOH(aq) by gas-phase OH-radicals. *J. Phys. Chem. A* **2014**, *118* (23), 4130−4137.
(75) Bagot, P. A. J.; Waring, C.; Costen, M. L.; McKendrick, K. G. Dynamics of Inelastic Scattering of OH Radicals from Reactive and Inert Liquid Surfaces. *J. Phys. Chem. C* **2008**, *112* (29), 10868−10877.
(76) Vlasenko, A.; George, I. J.; Abbatt, J. P. Formation of volatile organic compounds in the heterogeneous oxidation of condensed-phase organic films by gas-phase OH. *J. Phys. Chem. A* **2008**, *112* (7), 1552−1560.
(77) Pöschl, U.; Letzel, T.; Schauer, C.; Niessner, R. Interaction of Ozone and Water Vapor with Spark Discharge Soot Aerosol Particles Coated with Benzo[*a*]pyrene: O_3 and H_2O Adsorption, Benzo[*a*]-pyrene Degradation, and Atmospheric Implications. *J. Phys. Chem. A* **2001**, *105* (16), 4029−4041.
(78) Shiraiwa, M.; Garland, R. M.; Pöschl, U. Kinetic double-layer model of aerosol surface chemistry and gas-particle interactions (K2-SURF): Degradation of polycyclic aromatic hydrocarbons exposed to O_3, NO_2, H_2O, OH and NO_3. *Atmos. Chem. Phys.* **2009**, *9* (24), 9571−9586.
(79) Murphy, D. M.; Cziczo, D. J.; Hudson, P. K.; Thomson, D. S. Carbonaceous material in aerosol particles in the lower stratosphere and tropopause region. *J. Geophys. Res.: Atmos.* **2007**, *112* (D4), No. D04203.
(80) Power, R. M.; Simpson, S. H.; Reid, J. P.; Hudson, A. J. The transition from liquid to solid-like behaviour in ultrahigh viscosity aerosol particles. *Chem. Sci.* **2013**, *4* (6), 2597−2604.
(81) Berkemeier, T.; Shiraiwa, M.; Pöschl, U.; Koop, T. Competition between water uptake and ice nucleation by glassy organic aerosol particles. *Atmos. Chem. Phys.* **2014**, *14*, 12513−12531.
(82) Kuwata, M.; Martin, S. T. Phase of atmospheric secondary organic material affects its reactivity. *Proc. Natl. Acad. Sci. U. S. A.* **2012**, *109* (43), 17354−17359.
(83) Simoneit, B. R. T. Biomass burning—A review of organic tracers for smoke from incomplete combustion. *Appl. Geochem.* **2002**, *17* (3), 129−162.
(84) Cubison, M. J.; Ortega, A. M.; Hayes, P. L.; Farmer, D. K.; Day, D.; Lechner, M. J.; Brune, W. H.; Apel, E.; Diskin, G. S.; Fisher, J. A.; Fuelberg, H. E.; Hecobian, A.; Knapp, D. J.; Mikoviny, T.; Riemer, D.; Sachse, G. W.; Sessions, W.; Weber, R. J.; Weinheimer, A. J.; Wisthaler, A.; Jimenez, J. L. Effects of aging on organic aerosol from open biomass burning smoke in aircraft and laboratory studies. *Atmos. Chem. Phys.* **2011**, *11* (23), 12049−12064.
(85) Gross, S.; Iannone, R.; Xiao, S.; Bertram, A. K. Reactive uptake studies of NO_3 and N_2O_5 on alkenoic acid, alkanoate, and polyalcohol substrates to probe nighttime aerosol chemistry. *Phys. Chem. Chem. Phys.* **2009**, *11* (36), 7792−7803.
(86) Oja, V.; Suuberg, E. M. Vapor Pressures and Enthalpies of Sublimation of D-Glucose, D-Xylose, Cellobiose, and Levoglucosan. *J. Chem. Eng. Data* **1999**, *44* (1), 26−29.
(87) Xie, M.; Hannigan, M. P.; Barsanti, K. C. Gas/particle partitioning of 2-methyltetrols and levoglucosan at an urban site in Denver. *Environ. Sci. Technol.* **2014**, *48* (5), 2835−2842.
(88) May, A. A.; Saleh, R.; Hennigan, C. J.; Donahue, N. M.; Robinson, A. L. Volatility of organic molecular markers used for source

DOI: 10.1021/jp510489z
J. Phys. Chem. A 2015, 119, 4533−4544

apportionment analysis: Measurements and implications for atmospheric lifetime. *Environ. Sci. Technol.* **2012**, *46* (22), 12435−12444.
(89) Iinuma, Y.; Brüggemann, E.; Gnauk, T.; Müller, K.; Andreae, M. O.; Helas, G.; Parmar, R.; Herrmann, H. Source characterization of biomass burning particles: The combustion of selected European conifers, African hardwood, savanna grass, and German and Indonesian peat. *J. Geophys. Res.: Atmos.* **2007**, *112* (D8), No. D08209.
(90) Ziemann, P. J. Aerosol products, mechanisms, and kinetics of heterogeneous reactions of ozone with oleic acid in pure and mixed particles. *Faraday Discuss.* **2005**, *130*, 469−490.
(91) Knopf, D. A.; Anthony, L. M.; Bertram, A. K. Reactive uptake of O_3 by multicomponent and multiphase mixtures containing oleic acid. *J. Phys. Chem. A* **2005**, *109* (25), 5579−5589.
(92) Pfrang, C.; Shiraiwa, M.; Pöschl, U. Chemical ageing and transformation of diffusivity in semi-solid multi-component organic aerosol particles. *Atmos. Chem. Phys.* **2011**, *11* (14), 7343−7354.
(93) Springmann, M.; Knopf, D. A.; Riemer, N. Detailed heterogeneous chemistry in an urban plume box model: Reversible co-adsorption of O_3, NO_2, and H_2O on soot coated with benzo[*a*]-pyrene. *Atmos. Chem. Phys.* **2009**, *9* (19), 7461−7479.
(94) Kaiser, J. C.; Riemer, N.; Knopf, D. A. Detailed heterogeneous oxidation of soot surfaces in a particle-resolved aerosol model. *Atmos. Chem. Phys.* **2011**, *11* (9), 4505−4520.
(95) Zaveri, R. A.; Easter, R. C.; Schilling, J. E.; Seinfeld, J. H. Modeling kinetic partitioning of secondary organic aerosol and size distribution dynamics: Representing effects of volatility, phase state, and particle-phase reaction. *Atmos. Chem. Phys.* **2014** *14*, 5153−5181.
(96) Roldin, P.; Eriksson, A. C.; Nordin, E. Z.; Hermansson, E.; Mogensen, D.; Rusanen, A.; Boy, M.; Swietlicki, E.; Svenningsson, B.; Zelenyuk, A.; Pagels, J. Modelling non-equilibrium secondary organic aerosol formation and evaporation with the aerosol dynamics, gas- and particle-phase chemistry kinetic multilayer model ADCHAM. *Atmos. Chem. Phys.* **2014**, *14*, 7953−7993.
(97) de Gouw, J. A.; Warneke, C.; Parrish, D. D.; Holloway, J. S.; Trainer, M.; Fehsenfeld, F. C. Emission sources and ocean uptake of acetonitrile (CH_3CN) in the atmposhere. *J. Geophys. Res.* **2003**, *108* (D11), No. 4329.
(98) Koop, T.; Bookhold, J.; Shiraiwa, M.; Poschl, U. Glass transition and phase state of organic compounds: Dependency on molecular properties and implications for secondary organic aerosols in the atmosphere. *Phys. Chem. Chem. Phys.* **2011**, *13* (43), 19238−19255.
(99) Shiraiwa, M.; Pfrang, C.; Pöschl, U. Kinetic multi-layer model of aerosol surface and bulk chemistry (KM-SUB): The influence of interfacial transport and bulk diffusion on the oxidation of oleic acid by ozone. *Atmos. Chem. Phys.* **2010**, *10* (8), 3673−3691.
(100) Zhou, S.; Shiraiwa, M.; McWhinney, R. D.; Pöschl, U.; Abbatt, J. P. Kinetic limitations in gas-particle reactions arising from slow diffusion in secondary organic aerosol. *Faraday Discuss.* **2013**, *165*, 391−406.
(101) de Gouw, J. A.; Lovejoy, E. R. Reactive uptake of ozone by liquid organic compounds. *Geophys. Res. Lett.* **1998**, *25* (6), 931−934.
(102) Moise, T.; Talukdar, R. K.; Frost, G. J.; Fox, R. W.; Rudich, Y. Reactive uptake of NO_3 by liquid and frozen organics. *J. Geophys. Res.: Atmos.* **2002**, *107* (D2), No. 4014.
(103) Krieger, U. K.; Marcolli, C.; Reid, J. P. Exploring the complexity of aerosol particle properties and processes using single particle techniques. *Chem. Soc. Rev.* **2012**, *41* (19), 6631−6662.
(104) You, Y.; Renbaum-Wolff, L.; Carreras-Sospedra, M.; Hanna, S. J.; Hiranuma, N.; Kamal, S.; Smith, M. L.; Zhang, X.; Weber, R. J.; Shilling, J. E.; Dabdub, D.; Martin, S. T.; Bertram, A. K. Images reveal that atmospheric particles can undergo liquid-liquid phase separations. *Proc. Natl. Acad. Sci. U. S. A.* **2012**, *109* (33), 13188−13193.
(105) Shiraiwa, M.; Zuend, A.; Bertram, A. K.; Seinfeld, J. H. Gas-particle partitioning of atmospheric aerosols: Interplay of physical state, non-ideal mixing and morphology. *Phys. Chem. Chem. Phys.* **2013**, *15* (27), 11441−11453.
(106) Perraud, V.; Bruns, E. A.; Ezell, M. J.; Johnson, S. N.; Yu, Y.; Alexander, M. L.; Zelenyuk, A.; Imre, D.; Chang, W. L.; Dabdub, D.; Pankow, J. F.; Finlayson-Pitts, B. J. Nonequilibrium atmospheric secondary organic aerosol formation and growth. *Proc. Natl. Acad. Sci. U. S. A.* **2012**, *109* (8), 2836−2841.
(107) Wang, B. B.; Lambe, A. T.; Massoli, P.; Onasch, T. B.; Davidovits, P.; Worsnop, D. R.; Knopf, D. A. The deposition ice nucleation and immersion freezing potential of amorphous secondary organic aerosol: Pathways for ice and mixed-phase cloud formation. *J. Geophys. Res.: Atmos.* **2012**, *117* (D16), No. D16209.
(108) Molina, M. J.; Ivanov, A. V.; Trakhtenberg, S.; Molina, L. T. Atmospheric evolution of organic aerosol. *Geophys. Res. Lett.* **2004**, *31* (22), No. L22104.
(109) McNeill, V. F.; Yatavelli, R. L. N.; Thornton, J. A.; Stipe, C. B.; Landgrebe, O. Heterogeneous OH oxidation of palmitic acid in single component and internally mixed aerosol particles: Vaporization and the role of particle phase. *Atmos. Chem. Phys.* **2008**, *8* (17), 5465−5476.

DOI: 10.1021/jp510489z
J. Phys. Chem. A 2015, 119, 4533−4544